scientific reports

Check for updates

OPEN

Optimized production and fluorescent labeling of SARS-CoV-2 virus-like particles

Manon Gourdelier[1], Jitendriya Swain[1], Coline Arone[1], Anita Mouttou[1], David Bracquemond[1], Peggy Merida[1], Saveez Saffarian[2], Sébastien Lyonnais[3], Cyril Favard[1] & Delphine Muriaux[1,3]✉

SARS-CoV-2 is an RNA enveloped virus responsible for the COVID-19 pandemic that conducted in 6 million deaths worldwide so far. SARS-CoV-2 particles are mainly composed of the 4 main structural proteins M, N, E and S to form 100 nm diameter viral particles. Based on productive assays, we propose an optimal transfected plasmid ratio mimicking the viral RNA ratio in infected cells. This allows SARS-CoV-2 Virus-Like Particle (VLPs) formation composed of the viral structural proteins M, N, E and mature S. Furthermore, fluorescent or photoconvertible VLPs were generated by adding a fluorescent protein tag on N or M mixing with unlabeled viral proteins and characterized by western blots, atomic force microscopy coupled to fluorescence and immuno-spotting. Thanks to live fluorescence and super-resolution microscopies, we quantified VLPs size and concentration. SARS-CoV-2 VLPs present a diameter of 110 and 140 nm respectively for MNE-VLPs and MNES-VLPs with a concentration of 10e12 VLP/ml. In this condition, we were able to establish the incorporation of the Spike in the fluorescent VLPs. Finally, the Spike functionality was assessed by monitoring fluorescent MNES-VLPs docking and internalization in human pulmonary cells expressing or not the receptor hACE2. Results show a preferential maturation of S on N(GFP) labeled VLPs and an hACE2-dependent VLP internalization and a potential fusion in host cells. This work provides new insights on the use of non-fluorescent and fluorescent VLPs to study and visualize the SARS-CoV-2 viral life cycle in a safe environment (BSL-2 instead of BSL-3). Moreover, optimized SARS-CoV-2 VLP production can be further adapted to vaccine design strategies.

The Severe Acute Respiratory Syndrome Coronavirus-2 (SARS-CoV-2) is an emerging virus belonging to the *coronaviridae* family and the causative agent of the Coronavirus Disease 2019 (COVID-19). This respiratory virus emerged in China during the month of December 2019 and spread all around the world, leading to the ongoing pandemic declared in March 2020 by the World Health Organization (WHO). Pathogenicity of coronaviruses was previously observed during SARS-CoV and MERS outbreaks, which respectively occurred in 2002 and 2012. Concerning the current pandemic, COVID-19 has affected up to 460 million cases and caused 6 million deaths (WHO). It's demonstrating the importance of gathering knowledge on SARS-CoV-2 and developing vaccine design strategies. Among the possible strategies, Virus-Like Particles (VLPs) are high potential as they can be efficient and cheap vaccine candidates[1]. VLPs are multi-protein-lipid structures that mimic the organization and conformation of authentic native viruses without containing the viral genome.

To date, non-infectious VLPs have already been optimized using HIV-1 or Influenza structural proteins, allowing to study the entry and the assembly of these viruses in BSL-2 facilities. While the minimal requirement for HIV-1 VLPs uses only one viral protein, i.e. Gag[2], Kerviel and collaborators showed that the Influenza minimal system requires at least four proteins for VLPs production[3]. SARS-CoV-2 is an enveloped virus containing one RNA molecule and 29 proteins, including four structural proteins: membrane protein M, nucleoprotein N, envelope protein E and spike protein S[4]. Thus, determining the optimal combination (and proportion) of these structural viral proteins remains to be tested to obtain a minimal system for SARS-CoV-2 VLPs production.

Recently, research teams establish several minimal systems for SARS-CoV-2 VLPs production[5–11] exhibiting differences and contradictory results regarding the required structural viral proteins. Hence, different combinations regarding M, N, E and S were reported: the minimal system for VLPs production could require both M and

[1]Institut de Recherche en Infectiologie de Montpellier (IRIM), Université de Montpellier, CNRS UMR9004, Montpellier, France. [2]Department of Physics and Astronomy, Center for Cell and Genome Sciences, University of Utah, Salt Lake City, UT, USA. [3]CEMIPAI, Université de Montpellier, CNRS UAR3725, Montpellier, France. ✉email: delphine.muriaux@irim.cnrs.fr

E[5] or M, E and S[7] or M and E with N which plays a crucial role for VLPs formation[10] as previously reported for SARS-CoV[12]. A combination of M with N or S was also suggested[6]. Here, based on years of experiences in the production of HIV-1 Gag VLPs and their characterization using advanced microscopies[13–16], our work aims to revisit the minimal system for SARS-CoV-2 VLPs production. To optimize VLPs production from DNA plasmid ratio of M, N, E or S, we based our approach on viral RNA ratios obtained from transcriptomic analysis of the SARS-CoV-2 RNA genome in infected cells[17,18]. We also optimized the production of fluorescent VLPs (mono- or bi-color), made with tagged structural SARS-CoV-2 proteins, to create a valuable tool to image and study SARS-CoV-2 assembly and entry. We characterize these VLPs thanks to advanced microscopy methods such as Total Internal Reflection Fluorescence Microscopy (TIRF-M), Fluctuation Correlation Spectroscopy (FCS), correlative fluorescence-Atomic Force Microscopy (AFM) and Photo-Activable Localization Microscopy (PALM). These techniques allow us to determine the size, numbers and morphology of VLPs that we could compare to wild-type SARS-CoV-2 particles[19,20]. Finally, these fluorescent VLPs, made with tagged structural proteins (M or N) allowed us to evaluate the incorporation of the Spike and to follow viral particle internalization into host pulmonary cells, with or without the hACE2 receptor, using quantitative confocal microscopy.

Materials and methods

Cells and culture conditions. The HEK293T human embryonic kidney cell line was obtained from ECACC (Sigma-Aldrich, Germany) and maintained cultured in Dulbecco's modified essential medium (DMEM, Gibco) supplemented with 10% heat inactivated fetal calf serum (FCS, Thermo Fisher, USA), 50 U/mL of penicillin (Ozyme, France), 50 µg/mL of streptomycin (Ozyme, France), 1 mM sodium-pyruvate (Ozyme, France) and 25 mM of HEPES (Ozyme, France), at 37 °C with 5% CO_2.

Pulmonary A549 adenocarcinoma human alveolar basal epithelial cell lines[21] were obtained from ECACC (#86012804, Sigma-Aldrich, Germany) and cultured in Roswell Park Memorial Institute medium (RPMI) from Gibco supplemented with 10% heat-inactivated fetal calf serum (FCS, Thermo Fisher, USA), 50 U/mL of penicillin (Ozyme, France), 50 µg/mL of streptomycin (Ozyme, France), 1 mM sodium-pyruvate (Ozyme, France) and 25 mM HEPES (Ozyme, France), at 37 °C with 5% CO_2. The human pulmonary alveolar A549-hACE2 and A549-hACE2mScarlet stable cell lines were engineered using 2 different lentiviral vectors. For A549-hACE2, A549 cells were transduced with VSVg pseudotyped particles derived from a lentiviral vector from Flash Therapeutics (Toulouse, France) to express the human receptor ACE2. Cells were then sorted by flow cytometry (BD FACSAria™ III Cell Sorter) to obtain an A549-hACE2 population stably expressing hACE2. To detect hACE2, cells were washed twice in PBS and incubated for 1 h at 4 °C with primary goat antibody anti-human ACE2 protein (R&D AF933) (1:100). After washing in PBS, cells were stained 45 min at 4 °C with secondary antibody AF488-labeled donkey-anti-goat (Life technologies A11055) (1:3000) for 45 min. h-ACE2 expression was monitored in comparison with isotype control using NovoCyte Flow Cytometer (Agilent) (Supplemental Fig. 1A). For A549-hACE2-mScarlet, A549 were transduced with VSVg pseudotyped particles derived from lentiviral vector expressing mScarlet1 red fluorescent protein from Olivier Schwartz laboratory at Pasteur Institute (Paris, France) to express the human receptor hACE2mScarlet. Transduction efficiency was assessed by monitoring mScarlet1 expression (Maximum Excitation 569 nm/Maximum Emission 594 nm) using flow cytometry in comparison with A549 cells (Supplemental Fig. 1B).

DNA plasmids and cloning. The plasmid expressing Wuhan SARS-CoV-2 M protein, N protein, E protein and S protein were humanized and put under the control of the cytomegalovirus (CMV) promoter driven mammalian expression vectors as described in Swann et al.[7]. All the humanized M, N, E and S genetic sequences have been published in the supplemental material of Swann et al.[7], and are accessible via GenBank accession numbers. The SARS-CoV-2 M protein was tagged at the C-terminus placing the fluorescent protein within the lumen of the SARS-CoV-2 VLPs. To generate a functional tag, the following protein linker was used: Flex (Flexible protein linker): GGGGSGGGGSGGGGSGGGGD to generate both M-Flex-mCherry and M-Flex-GFP. The plasmids were generated by the synthesis of Flex-mCherry and Flex-eGFP and inserted into humanized M plasmids described in[7] using EZcloning from Genscript. The SARS-CoV-2 N protein was tagged at the N-terminus. The GFP and mEOS2 tags were amplified by PCR from peGFP and pmEOS2 using *Pfu* Polymerase (M7741, Promega), dNTP mix (10297018, Thermo Scientific) and primers designed to carry NheI and KpnI restriction sites (Sigma Aldrich). PCR amplified inserts were added at the N-terminus of N protein in pcDNA3.1 + plasmid, and purified with the NucleoSpin Gel and PCR Clean-up kit (Macherey–Nagel). The plasmid N and inserts were digested and purified. Ligation between these digested products was performed using T4 DNA ligase (M0202S, NEB). 50 µL of competent bacteria were next transformed with 5 µL of the ligation reaction product. Plasmids were extracted from various colonies with the NucleoSpin plasmid mini-kit (740,588.50, Macherey–Nagel). Validated plasmids were then sequenced by Eurofins.

DNA transfection. HEK293T cells were seeded into a 6-well plate or 10 mL dishes 24 h before transfection. Plasmids expressing viral proteins were transfected with $CaCl_2$/HBS2X (50 mM HEPES pH 7.1, 280 mM NaCl, 1.5 mM Na_2HPO_4) (v/v) into HEK293T cells. A total of 1.4 µg of mixed plasmids was applied for the transfection of a well (for 6-well plate) and 0.7 µg/well for individual plasmid. Co-transfection of double, triple or quadruple plasmids was conducted with M, N, E and S with plasmid ratio 3:3:3:5 respectively (0.3 µg:0.3 µg:0.3 µg:0.5 µg per well to 6-well plate for example) in the first assay as shown in Fig. 1B. Optimization of SARS-CoV-2 VLPs was performed by co-transfecting M, N, E and S with a plasmid ratio of 3:12:2:5 respectively corresponding to the molecular viral RNA ratio found in infected cells[17,18], corresponding, for an example, to a total of 2,2 µg/well of 6 well plate (with M:N:E:S corresponding to 0.3 µg:1.2 µg:0.2 µg:0.5 µg of transfected plasmid) as shown in Fig. 1C. Optimization of fluorescent SARS-CoV-2 VLPs production was performed by co-transfecting M, M(GFP) or

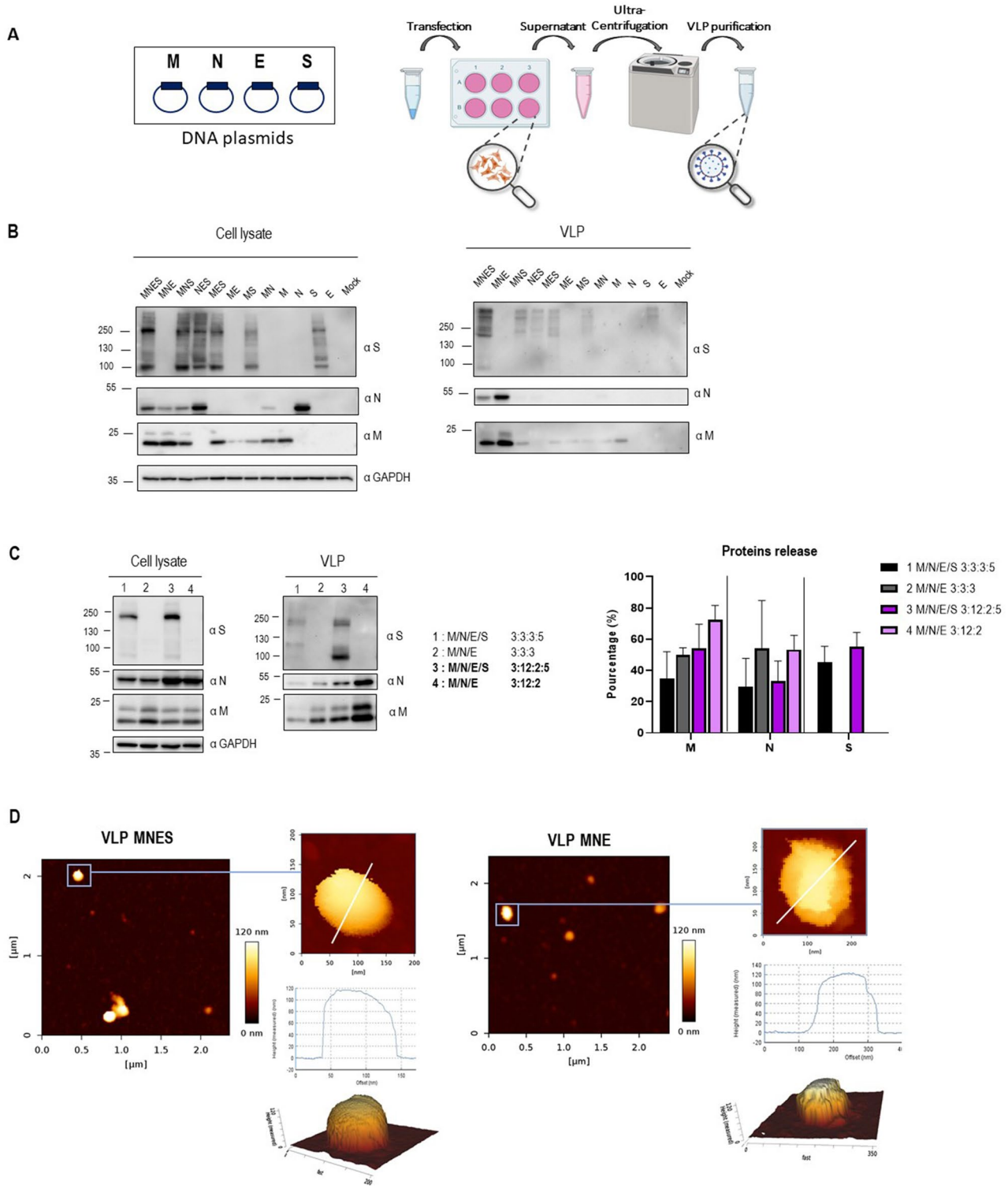

Figure 1. Optimization of SARS-CoV-2 VLPs assembly and particle analysis using immunoblots and atomic force microscopy imaging. (**A**) Scheme of VLPs production and purification. Thanks to BioRender for images. (**B**) Western blot of cell lysates and VLPs of HEK293T cells transfected with M, N, E or S as indicated for each lane. The transfected M/N/E/S plasmid ratios are respectively MNES 3:3:3:5; MNE 3:3:3; MNS: 3:3:5, NES 3:3:5, MES 3:3:5, ME 3:3, MS 3:5, M 3, N 3, E 3, S 5. N = 1. (**C**) Western blot of cell lysates and VLPs of HEK293T cells transfected with the indicated 3:3:3: ± 5 and 3:12:2: ± 5 M, N, E ± S transfected plasmid ratios. Right panel: Graph representing the percentage of M, N, E and S in released VLPs after quantification of the western blot band intensities for each condition. N = 3 independent experiments. (**D**) AFM imaging of SARS-CoV-2 MNES VLPs and MNE VLPs using quantitative QI mode AFM in TNE buffer. For each condition, a topographic image of 2.5 µm × 2.5 µm and zoom of a particle is shown, with a 3D projection. The color gradient for the Z scale is the same for all panels. The topographical profile plots along the white line are shown for each VLP. N = 2 with 18 VLP analyzed.

M(mCherry), N, E and S with plasmid ratio of 2:2:12:2:5 respectively, and M, N, N(GFP) or N(mEOS2), E and S with plasmid ratio of 3:9:3:2:5 respectively. Then, transfected cells were washed 6 h later with phosphate-buffered saline (PBS 1x) and harvested 24 h to 48 h post-transfection with Exofree medium. Attached cells were washed with PBS, harvested, centrifuged at 1500 rpm for 5 min at 4 °C and lysed with RIPA lysis buffer (25 mM Tris HCl pH 7.6, 150 mM NaCl, 1% NP-40, 1% sodium deoxycholate, 0.1% SDS) (ThermoFisher) supplemented with protease inhibitor cocktail (Sigma). Following centrifugation at 15,000 rpm for 10 min at 4 °C, cell lysates were collected. The protein concentrations in cell lysates were estimated using Bradford assays. Under each condition, the percentage of cell viability was measured by trypan blue cell counting before cell lysis.

Collected VLPs and purification. VLPs were obtained from culture medium of transfected cells by clarification at 5000 rpm for 5 min at 4 °C. Then the VLPs were collected from clarified supernatants after ultracentrifugation, through a 25% sucrose cushion in TNE buffer (10 mM Tris–HCl pH 7.4, 100 mM NaCl, 1 mM EDTA), at 28,000 rpm or 30,000 rpm for 3 h at 4 °C in Beckman SW41Ti or SW55Ti rotors respectively depending on the volume. VLPs from ultracentrifugation were resuspended overnight at 4 °C in TNE buffer. The purified VLPs were stored at 4 °C.

Antibodies. Immunoblotting were performed by using the following antibodies: rabbit anti-M 1:1000 (100-401-A55, Rockland TEBU-BIO); rabbit anti-N 1:3000 (200-401-A50, Rockland TEBU-BIO); mouse anti-S 1:1000 (GTX632604, Genetex); anti-GAPDH antibody coupled to HRP 1:25,000 (G9295, Sigma). For immunospotting, rabbit anti-Spike neutralizing Antibody 1:100 (40592-R001, Sino Biological), mouse anti-CD81 1:100 (sc7637, 1.3.3.22, Santa Cruz), fluorescent rabbit Alexa555 and mouse Alexa647-conjugated secondary antibodies 1:2000 (Invitrogen) were used in this study.

Immunoblotting. Proteins from cell lysates (20 µg of total proteins) or VLPs (volume to volume) were loaded and separated on 8% and 12% SDS-PAGE gel and transferred onto a polyvinylidene difluoride transfer membrane (Thermo Fisher). Immunoblotting was performed by using the corresponding antibodies. Horse Radish Peroxidase signals were revealed by using Amersham ECL Prime (Sigma Aldrich). Images were acquired using the Chemidoc Imaging system (Bio-Rad). Each band intensity on the immunoblot was quantified using the ImageJ software. Quantification was established by the following formula for each viral protein: VLP/(VLP + cell lysate) relative to GAPDH as a loading control.

Atomic force microscopy on VLPs. Glass-bottom FluoroDish Cell Culture dishes (WPI) were coated with 0.01% poly-L-lysine (Sigma) for 30 min at room temperature and rinsed three times with 1 mL of PBS (Thermo Fisher Scientific). Purified MNES, MNE, M(GFP)NES and M(GFP)NE VLPs were diluted 10 times in 100µL TNE buffer and were deposited for 30 min at room temperature on the coated dishes for adsorption. Dishes were next filled with 2 mL PBS 1X. AFM imaging was performed at room temperature on a NanoWizard IV atomic force microscope (JPK BioAFM, Bruker Nano GmbH, Berlin, Germany) mounted on an inverted microscope (Nikon Ti-U, Nikon Instruments Europe B.V, Amsterdam, the Netherlands) equipped with a standard monochrome CCD camera (ProgRes MFCool, Jenoptik, Jena, Germany). Fluorescence imaging was performed by wide-field illumination (Intensilight Hg lamp, Nikon) with a 100X objective (Nikon CFI Apo VC, 1.4 NA, oil immersion) and the appropriate filter cube for GFP fluorescence (Ex 466/40, DM 495, BA 525/50). A software module (DirectOverlay, JPK Bio-AFM, Bruker Nano GmbH, Berlin, Germany) was used to calibrate the tip position with the optical image. AFM topographic images were obtained in TNE using the quantitative imaging (QI) mode with BL-AC40TS cantilevers (mean cantilever spring constant kcant = 0.1 N/m, Olympus). Before each set of acquisitions, the sensitivity and spring constant of the cantilever were calibrated (thermal noise method). The applied force was kept at 200 pN with a constant approach/retract speed of 25 µm/s (z-range of 100 nm). Using the JPK SPM-data processing software, images were flattened with a polynomial/histogram line fit. Low-pass Gaussian and/or median filtering was applied to remove minor noise from the images. The Z-color scale in all images is given as relative after processing. Particle height analysis, based on the height (measured) channel of the QI mode, was performed using the cross-section tool of the analysis software to calculate the maximal central height of each particle.

Fluorescence correlation spectroscopy on fluorescent VLPs. Glass coverslips were coated with 0.01% poly-L-lysine (Sigma) for 30 min at room temperature and rinsed three times with 1 mL of PBS (Thermo Fisher Scientific). Purified M(GFP)NES and M(GFP)NE VLPs were diluted 10 times in 100µL TNE buffer and were deposited for 30 min at room temperature on the coated dishes for adsorption. Experiments were conducted on a Zeiss LSM780 confocal microscope. The 488 nm excitation laser beam is focused onto the sample using a water immersion objective (40x, NA = 1.20) resulting in a 210 nm laser waist (ω_0) in the object plane as calibrated using Rhodamine 6G in water at 25 °C (with D = 280 µm^2/s). When considering a Gaussian profile for illumination (ω_z/ω_0=5), an effective volume (Vo) of ~ 0.3 fL is obtained, since the sample fluorescence is collected through a confocal pinhole (fixed at 1 Airy unit). Fluorescence intensity fluctuations traces (at least 120) were recorded for 10 s and correlated immediately with the built-in Zen software.

Correlograms are then fitted with the PyCorrFit software[22] using a classical 3D free diffusion model

$$G(\tau) = \frac{1}{N}\left(1 + \frac{\tau}{\tau_D}\right)^{-1}\left(1 + 25\frac{\tau}{\tau_D}\right)^{-1/2} \quad (1)$$

in order to obtain the diffusion time τ_D and the number of particle N (Eq. 1). All particles were assumed to have similar brightness.

The VLPs concentration (in particle number/mL) is immediately obtained by Eq. (2)

$$c = \frac{N}{V_0} \tag{2}$$

The VLPs diameters (d) were calculated using the following expression:

$$d = \frac{4k \cdot T\tau_D}{3\pi \cdot \mu \cdot \omega_0^2} \tag{3}$$

with τ_D diffusion time, obtained by fitting the experimental correlograms with Eq. (1), ω_0 the laser waist, k the Boltzmann constant, T the temperature in Kelvin and μ the dynamic viscosity of the buffer.

photo-activated localization microscopy (PALM) on photoswitchable VLPs. Glass coverslips were coated with 0.01% poly-L-lysine (Sigma-Aldrich) for 30 min at room temperature and rinsed three times with 1 mL of PBS (Thermo Fisher Scientific). Purified MN(mEOS2)E VLPs and N(mEOS2) particles were diluted 10 times in 100μL TNE buffer and were deposited for 30 min at room temperature on the coated dishes for adsorption. Images were acquired in TIRF mode on an inverted microscope (Nikon Instruments Europe B.V, Amsterdam, the Netherlands) using a NA 1.49 SR-100 × TIRF objective at room temperature. A 561 nm laser was used to excite the 405 nm photo-convertible mEOS-2 protein. The fluorescence is collected through a dedicated cube containing a dichroic mirror and an emission bandpass filter centered at 617 ± 73 nm. 20,000 images were captured by an iXon U897 camera from Andor at a rate of 50 Hz. PALM acquisitions were analyzed using the ThunderSTORM plugin in Fiji[23]. The module DBSCAN of the super-resolution quantification software SR Tesseler[24] was used to quantify cluster diameters.

Immuno-spotting assay on VLPs. FluoroDish cell culture Petri Dishes (WPI, USA) were coated overnight at room temperature with 0.01% poly-L-lysine (Sigma) and rinsed three times with PBS. Purified fluorescent SARS-CoV-2 VLPs were diluted 10 times in TNE buffer and 100 µL were deposited 30 min at room temperature on the poly-L-lysine coated dish for adsorption. PFA 4% was deposited 15 min at room temperature for fixation. NH_4Cl was added for 5 min at room temperature. Dishes were rinsed once with BSA 3%PBS and were blocked with BSA 3%PBS for 15 min at room temperature. Immuno-spotting was performed by using corresponding antibodies. After incubation, dishes were rinsed three times with PBS and stored at 4 °C. Then, images of fluorescent VLP were acquired using the TIRF-Microscopy (Nikon) with the 100 × objective. 13 Images corresponding to 250–300 fluorescent VLPs were analyzed by ImageJ/Fiji software and ComDet Plugin was used for quantifying the number of fluorescent VLPs and the double GFP/mCherry colocalization. The image background was estimated at 10% of the fluorescent intensity signal of VLPs and was removed from images before colocalization quantification.

Fluorescent VLPs internalization assay. VLPs internalization assays were performed using fluorescent M(GFP)NE and M(GFP)NES particles or MN(GFP)ES VLPs. Human pulmonary A549 or A549-hACE2 cells were harvested live in cold PBS 1x (after 24 h in culture on glass coverslip). M(GFP)NE or M(GFP)NES or MN(GFP)ES VLPs were diluted (1:20) in transparent L15 Solution (Gibco) and put into contact with the live cells. The cells were then incubated either at 37 °C for 15 min or at 4 °C for 1 h. Unbound VLPs were removed by washing cells 3 times with cold PBS 1x. The cells were then fixed with 4% PFA and mounted with Prolong Gold antifade reagent with DAPI (Invitrogen) for confocal imaging. Confocal fluorescence images were generated using a CD7 confocal laser-scanning microscope (Zeiss, Germany) equipped with a 50 × 0.5 ×, 1.2 NA oil objective or with a LSM980 confocal laser-scanning microscope (Zeiss, Germany) equipped with a 63 × 1.4 NA oil objective. The cells were imaged as Z stack with 0.3 µm sections and deconvoluted using Deconvolution lab plugin in Fiji with a theoretical PSF. Fiji was also used to count the number of MN(GFP)ES VLP (ie. Fluorescent dots) per cell.

To measure VLP distance from cell center, using Icy, we first performed a Z-projection of stacks, then segmented the cells to establish their center position and subsequently performed cell center/M(GFP)-VLP distance measurements.

Statistical analyses. Statistical analyses were performed using Origin 8.5 and Graph Pad prism softwares. ANOVA and t-tests were used for the statistical comparison of data.

Graph Pad. Graph Pad was used for performing graphs.

Results

Optimized virus-like-particles production by mimicking SARS-CoV-2 RNA ratio. We first explored the minimal system requirements for SARS-CoV-2 VLPs production. We played with combination of plasmids expressing M, N, E or S (under the same CMV promoter), transfected individually, by pairs or with a plasmid ratio of 3:3:3:5. Transfections were performed on the highly productive HEK293T cell lines, widely used in VLPs production[3,5–7,10]. At 48 h post-transfection, VLPs released in cell supernatants were purified by ultracentrifugation over a 25% sucrose cushion in TNE buffer (Fig. 1A). Viral proteins in cell lysates and in

the purified VLPs were next analyzed by western blot, and the percentage of protein released was calculated (Fig. 1B). The results show that only the combination of M, N and E proteins was able to efficiently release VLPs 48 h post-transfection. None of the single or dual combinations generated particle production. Without E, some MNS particles were pelletable but the efficiency dropped by 2.5 fold. Without M or N, no VLP was produced in our conditions (Fig. 1B). Thus, it appears that the interaction between M and N is absolutely required for VLP production. The combination of M, N, E and S could also produce VLPs incorporating S (Fig. 1B, central panel), but with a reduction of N proteins in comparison with the MNE combination. In all conditions, cell viability was not impacted (Supplemental Fig. 2), indicating that the released particles are not coming from dead cells, and are indeed secreted VLPs. The VLPs production occurred only upon the combination MNE, with or without S, indicating that S is dispensable for SARS-CoV-2 VLPs production (Fig. 1B, right panel). Contrary to other recent reported studies[5,7,8], ME or MES combinations were not sufficient to form VLPs in our condition. We next evaluated VLPs production using plasmid ratios mimicking the wild-type SARS-CoV-2 mRNA ratio (extracted from RNAseq data of infected cells[17,18]) coding for the 4 main structural proteins. For that, the expression of M, N, E and S is under the same CMV promotor, with a respective 3:12:2:5 ratio. This transfected plasmid ratio was compared with the arbitrary MNES ratio 3:3:3:5 (Fig. 1C). Interestingly, the ratio MNE 3:12:2 was found optimal for the production of SARS-CoV-2 VLPs, with a 1.5-fold increase of M incorporation (Fig. 1C, in the graph compare the % of M release 50 ± 4—lane 2—with 72 ± 9—lane 4), but no change in N incorporation (compare the % of N release 54 ± 30 with 55 ± 9), as compared to the MNE 3:3:3 ratio (Fig. 1C, graph). The expression of S decreased the amount of N and M proteins incorporated in VLPs by 1.5 fold (Fig. 1C, graph, compare the % of M release 72 ± 9 versus 54 ± 15 with S, and, for N, compare 55 ± 9 versus 33 ± 12 with S), suggesting that S modulates the incorporation of N or M most probably due to its own incorporation. Altogether, these data establish that the minimal system for SARS-CoV-2 VLPs production is composed of M, N and E structural viral proteins. The presence of S for VLPs production is optional, but when expressed, S may be incorporated in the VLP accompanied by a diminution of N and M proteins incorporation. However, the incorporation of S on the pellet VLPs is greater when the transfected plasmid ratio was 3:12:2:5 rather than 3:3:3:5 (see graph Fig. 1C, compare the % of S release, 55 ± 9—lane 3—to 45 ± 10—lane 1, respectively). Furthermore, the striking difference was coming from S maturation: the maturation of S into S2 was much more efficient when the ratio was respecting the 3:12:2:5 proportionality (Western Blot Fig. 1C, compare S2 in lanes 1 and 3 "VLP"). This suggests that the production of mature SARS-CoV-2 particles is most probably fine-tune regulated by viral RNA ratios during infection[17], and thus viral protein assembly.

The purified MNE and MNES VLPs were next imaged by AFM in the buffer for size and shape characterization (Fig. 1D), in the conditions previously used for the wild-type virus[19]. MNE and MNES VLPs appeared as spherical particles, with shapes similar to those of WT-SARS-CoV-2 particles. As seen previously reported with the wild-type virus, AFM in liquid in standard scanning mode did not resolved the S proteins at the surface of the MNES VLPs, which has been attributed to the fast dynamics of S in the envelope. The mean height of the VLP was 112 ± 48 nm for MNE and 126 ± 17 nm for MNES, showing a ~ 25% increase in size as compared with wild-type SARS-CoV-2 particles analyzed by AFM[19,25] and electron microscopy (EM)[26,27]. Recent literature on SARS-CoV-2 VLPs reported a size around 100-200 nm in diameter either using AFM[7] or EM[5–7,9].

Production of fluorescent SARS-CoV-2 VLPs by tagging M and N proteins. We next aimed at producing fluorescent SARS-CoV-2 VLPs from transfected HEK293T cells, by co-transfecting a M(Cter-GFP) fusion protein together with M, N and E, with a ratio M/M(GFP) of 2:2, supplemented or not with S. That way, M(GFP) incorporation into VLPs was possible and the protein incorporation was verified by Western Blot in both MNE and MNES conditions (Fig. 2A, Supplemental Fig. 2). Results indicated an incorporation of M(GFP) in the MNE and MNES VLPs. The purified fluorescent VLPs fraction was deposited on glass coverslips and fluorescent particles were successfully detected using Total Internal Reflexion Fluorescence (TIRF) Microscopy (Fig. 2B), for either M(GFP)NE or M(GFP)NES VLPs. Fluorescent spots were not detected in the control (Mock) purified from cells only transfected with M(GFP) suggesting that M(GFP) is indeed incorporated in VLPs. Furthermore, correlative fluorescence/AFM imaging confirmed that these fluorescent dots (Fig. 2C) are VLPs of shape and size similar to the unlabeled VLPs (Fig. 1D); therefore demonstrating the production of M(GFP)NE or M(GFP)NES VLPs incorporating M(GFP). It is worth noticing that not all the particles found by AFM were GFP(+) indicating that a fraction of the VLPs produced are not labeled or that the smaller size particles are not VLPs but rather extracellular vesicles (Fig. 2D). In comparing particle size distribution by AFM, we can notice that all the particle of size superior to 90 nm in height were GFP(+) and that below 90 nm in height, smaller particles were never GFP(+) and similar in size to the extracellular vesicles secreted from the cells that do not express any SARS-CoV-2 proteins (Fig. 2D, compare MNES/MNE with Mock conditions).

We then determined the M(GFP)NES and M(GFP)NE VLPs size and approximate concentration using Fluorescence Correlative Microscopy (FCS) (Fig. 2D). GFP(+) particle concentration of 5.10^{12} to 7.10^{12} particles/ml were found respectively for M(GFP)NES and M(GFP)NE VLPs suggesting a very efficient production considering that not all the VLPs are labeled with GFP. Interestingly, we were able to differentiate VLPs sizes, measuring diameters of 120 ± 10 nm (mean ± sd) for VLPs without S and 140 ± 20 nm for VLP with S (Fig. 2E). The latter particle size might correspond to the VLPs with Spikes. This result is also nicely consistent with the average diameter of VLPs obtained by AFM.

To accurately measure particle size with single-molecule localization microscopy, we next designed and produced mEOS2 photoconvertible fluorescent protein SARS-CoV-2 VLPs using a fusion N(Nter-mEOS2) protein. These photoconvertible VLPs were used to perform Photo-Activated Localization Microscopy (PALM) to provide another estimation of their size[14,15]. We directly compared these sizes with the particles released into the cell supernatant from cells only transfected with N(mEOS2). The results are shown in Fig. 2E. MN(mEOS2)

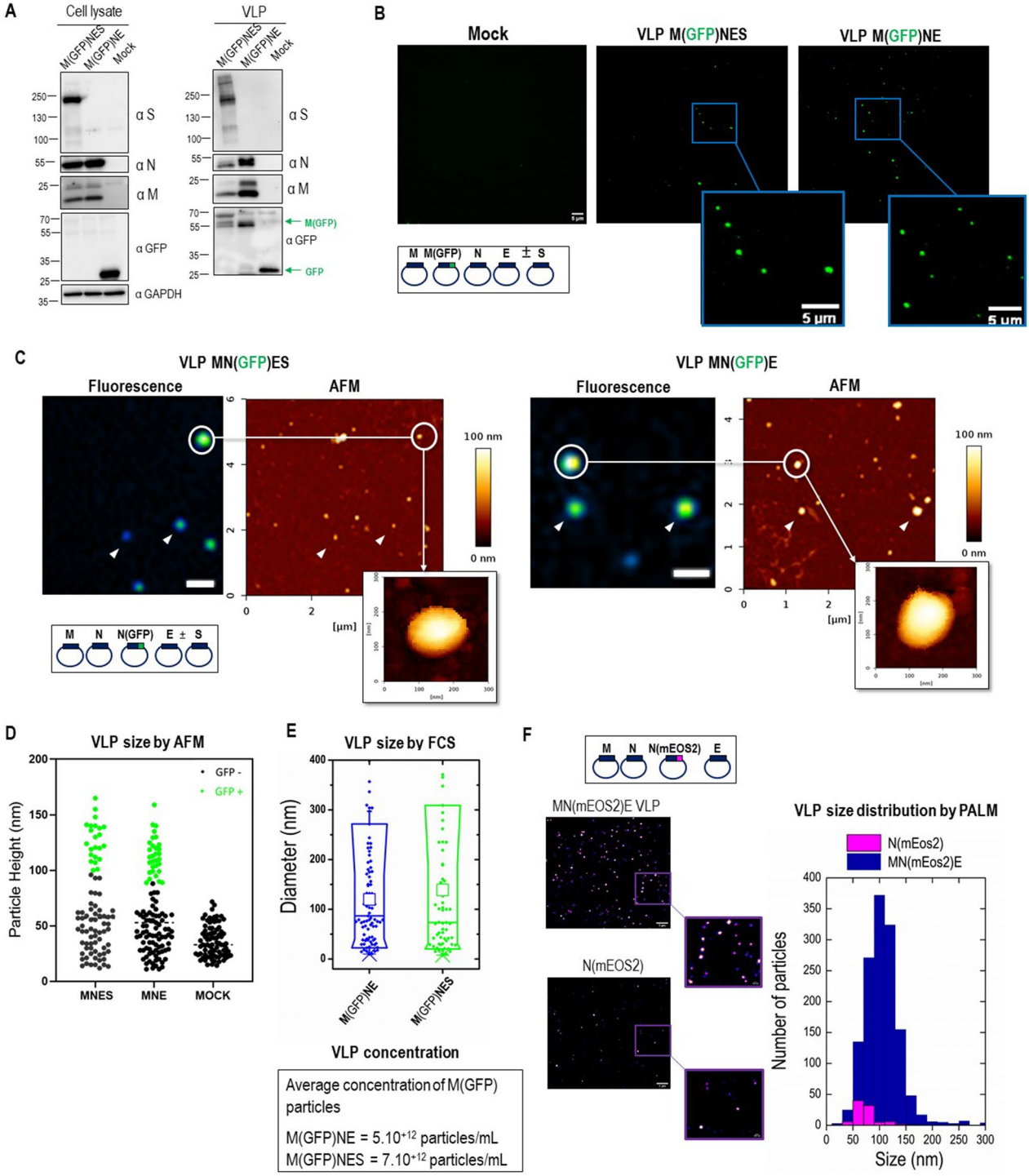

Figure 2. Size and concentration of fluorescent and photoconvertible SARS-CoV-2 VLPs. (**A**) Western blot of cell lysates and VLPs of HEK293T cells transfected with M/M(GFP), N, E ± S with the optimal plasmid ratio of M/M(GFP):N:E ± S as 2/2:12:2 ± 5. (**B**) TIRF microscopy images of SARS-CoV-2M(GFP)NE and M(GFP) NES VLPs were deposited on a glass coverslip. The scale bar is 5 µm. (**C**) Correlative AFM and wide-field fluorescence images of fluorescent SARS-CoV-2 MN(GFP)E and MN(GFP)ES VLPs. Scale bars represent 1 µm. (**D**) AFM Size (particle height) distribution of all particles adsorbed on the surface in the MN(GFP)ES and MN(GFP)E VLPs preparations versus the mock control (extracellular vesicles naturally released from the transfected cells). The number of particles counted were 86, 81 and 84 respectively. The GFP+ particles found by correlative AFM are indicated as green dots. (**E**) The size and concentration of M(GFP)NE and M(GFP) NES VLPs are determined by FCS. (**F**) Images and quantitative size distribution of MN(mEOS2)E VLPs and N(mEOS2) particles using super-resolution PALM microscopy. All these experiments were done twice with more than several hundred of particles analyzed in each condition.

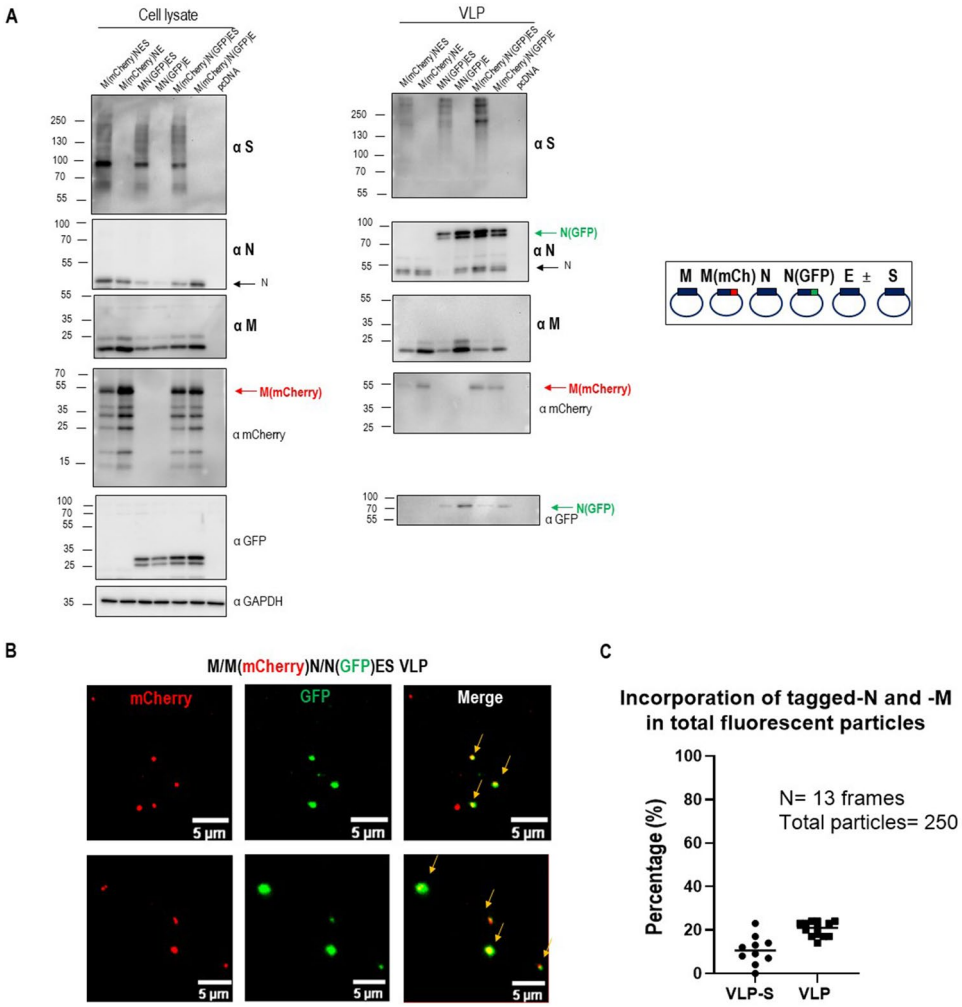

Figure 3. Description of dual-color fluorescent SARS-CoV-2 VLPs with tagged-M and -N incorporation. (**A**) Western blot of cell lysates and VLPs of HEK293T cells transfected with M, M(mCherry), N, N(GFP), E and S with the optimal ratio of M/M(mCherry)/N/N(GFP)/E ± S plasmids 2/2:9/3:2 ± 5. (**B**) Images of dual-color SARS-CoV-2M(mCherry)N(GFP)E ± S VLPs using TIRF Microscopy. Arrows show dual-color VLPs. The scale bar is 5 µm. (**C**) Quantitative colocalization of dual color GFP/mCherry VLPs using ComDet plugin in ImageJ. For each condition, 250–300 fluorescent particles were counted over 13 images (frames). One point in the graph represents the % of GFP/mCherry colocalization in one frame. N = 2, 250 particles analyzed.

E VLPs exhibited a 108 ± 1 nm (mean ± sem) diameter with a high number of particles observed in the field of view (N ~ 1300) while the N(mEOS2) particles were much less numerous (N ~ 60) with a significantly smaller diameter (78 ± 3 nm). This result confirms that SARS-CoV-2 VLPs are on average 100 nm diameter in size no matter the technic used thus slightly bigger than the wild-type virus. Secondly, the fact that N alone is being released inefficiently (20 fold less) than the MNE combination confirms that MN(mEOS2)E is efficiently producing photoactivable VLPs (Fig. 2F, graph of particle size distribution). Overall, our results show the successful incorporation of fluorescent M or N tagged proteins in MNE and MNES VLPs, with a ratio of labeled/unlabeled viral proteins of 1:1 or 1:3 respectively, suggesting that this incorporation does not impair VLPs assembly, as it was previously reported for the generation of fluorescent HIV-1 Gag VLPs[13–16]. Dual color fluorescent labeled VLPs were next tried to challenge the limit of fluorescent tags incorporation into the VLPs. Dual color VLPs were produced by co-expression of M(Cter-mCherry) and N(Nter-GFP) with M, N and E supplemented or not with S in transfected HEK293T cells (Fig. 3). M(mCherry) and N(GFP) incorporation into VLPs collected 48 h post-transfection was verified by Western Blot (Fig. 3A, Supplemental Fig. 2). Figure 3A exhibits 2 bands at molecular weights of approximately 80 and 105 kDa, corresponding to respectively fluorescently (GFP or mCherry, ~ 26 kDa) tagged M (~ 55 kDa) and tagged N proteins (~ 80 kDa). Two color TIRF images of these dual color VLPs showed the presence of a mix of GFP(+) or mCherry(+) single labeled VLPs as well as particles containing the two fluorescent labels (Fig. 3B). A total of 250–300 fluorescent particles were counted over 13 images (frames) on which we evaluated the percentage of particles only mCherry(+) or only GFP(+). The results showed that half of the fluorescent VLPs were N(GFP)(+) and half were M(mCherry)(+) in the case of MNE VLPs but only one-third were N-GFP(+) in the case of MNES VLPs, indicating that upon S incorporation in the VLPs, less

N(GFP) was incorporated. The colocalization of the dual color GFP/mCherry VLPs was also quantified, which allowed us to monitor the relative incorporation of M(mCherry) and N(GFP) in a VLP (Fig. 3C). We quantify that only 20 ± 3% and 11 ± 7% of the VLPs are dual color containing M(mCherry) and N(GFP) in the same MNE and MNES VLPs respectively (Fig. 3C) when mixing label and unlabeled proteins. This indicates that VLPs could incorporate the two fluorescent labeled M and N proteins without impairing assembly. We also tried to produce M(mCherry)N(GFP)E VLP, i.e. in the presence of both tagged M and N, but this was totally preventing VLPs production (data not shown). Since the fluorescent protein tag is located at the C-ter of M and N-ter of N, it should be located inside the VLP. Only when mixing both label and unlabeled proteins at a ratio of 1:1 for M or at a ratio of 3:9 for N(GFP) versus N, then production of labeled particles was possible. However, in both cases, we can notice that the incorporation of S in the fluorescent VLPs was mainly in its immature uncleaved form (Supplemental Fig. 2D,E) as compared to VLP without fluorescent proteins (Supplemental Fig. 2C) indicating that the intra-lumenal GFP or mCherry of the N- or M-tagged proteins do not interfere with S incorporation in VLP but prevent its correct maturation, impairing S/S2 cleavage site and probably its conformation, questioning the correct assembly of these particles in that case. Thus, in order to produce fluorescent MNES-VLPs with an optimal maturation and cleavage of the Spike, we evaluated the best ratio between unlabeled N and labeled N(GFP) to produced fluorescent VLPs. Western blots show that at a ratio of 3:1 or 4:1 of N/N(GFP), the Spike is efficiently incorporated and matured as in unlabeled MNES VLPs (Supplemental Fig. 3).

Quantitative imaging of S incorporation in fluorescent VLPs. Furthermore, to estimate the Spike incorporation on fluorescent VLPs, we used the M(GFP)NES fluorescent VLPs to quantify the percentage of GFP labeled VLP incorporating S by immuno-spotting coupled to TIRF microscopy, using an anti-S neutralizing antibody and an AlexaFluor555 secondary antibody (Fig. 4A). Non-specific binding of the anti-S antibody/secondary antibody was 6 ± 6% on the M(GFP)NE VLPs, while the absence of VLP did not show any significative background (less than 1% for "no VLP"). Quantification of fluorescent red/green dot spots colocalization indicated that 27 ± 12% of the M(GFP)NES VLPs incorporated S (Fig. 4B). Although, since some VLPs were not GFP labeled, "red" dots also appeared. To prove that these dots were more likely VLPs rather than exosomes/extracellular vesicles (EVs) containing S, we checked the colocalization between these "red" S dots and CD81 with an anti-CD81 exosomal marker (Supplemental Fig. 4) using the same immuno-spotting assay. Less than 10% of the "red" dots containing only S were colocalizing with CD81 and none of the M(GFP)NES VLPs were CD81 positive, suggesting that M(GFP)NES VLPs are a mixture of GFP(+)VLPs and unlabeled VLPs containing S but not CD81 EVs. Our results show that the Spike S is well incorporated on MNES VLPs with or without M-GFP (Fig. 4B), suggesting that S incorporation is mainly driven by MNE confirming the results seen by immunoblotting (Fig. 1B). We also checked that these VLPs were distinct from CD81(+) extracellular vesicles (Supplemental Fig. 4). On the other hand, not all the VLPs-(M-GFP) were carrying the Spike, suggesting that part of the fluorescent VLPs assemble without S.

In order to estimate the incorporation of the other viral proteins N and M with the N(GFP) and M(GFP) tagged proteins, respectively, we performed the same immuno-spotting assay with anti-N and anti-M antibodies on MN(GFP)NES and M(GFP)MNES VLPs (Fig. 4C) and quantified the incorporation of N and M in the respective fluorescent VLPs (Fig. 4D). Results show that 73 ± 5% of M is colocalizing with M(GFP)VLPs and 95 ± 1% of N with N(GFP)VLPs in contrast to S (20 ± 4% in N(GFP) VLPs). Overall, these results suggest a better incorporation of N/N(GFP) tagged protein rather than M(GFP) in fluorescent VLPs and that not all the fluorescent VLPs contain the Spike.

Internalization of the fluorescent SARS-CoV-2 VLPs in host pulmonary cells. In order to study the functionality of the Spike incorporated in the fluorescent VLPs, we performed an internalization assay of the SARS-CoV-2 M(GFP) or N(GFP) tagged VLPs. To do so, M(GFP)MNE VLPs versus M(GFP)MNES VLPs were incubated with pulmonary A549 cells expressing the human receptor hACE2 (Supplemental Fig. 1). The internalization of both fluorescent VLPs, M(GFP)NE versus M(GFP)NES, was monitored at 37 °C (active endocytosis) or at 4 °C (partially blocked endocytosis). A difference in internalization between M(GFP)NES VLPs and M(GFP)NE VLPs was observed and revealed using quantitative confocal microscopy (Fig. 5A). To quantify this difference, we measured the distances (d_1,d_2,…d_n) of VLPs, identified as GFP bright dots, to the center of the cell (Fig. 5B), this cell center being the intercept of the major and minor axis (r_1 and r_2), established for each cell. As these radii represent the mean longest (r_1) and shorter (r_2) distances between the cell border and the cell center, it suggests that every VLP distance that will be found in between these two radii corresponds to a VLP located at the border of the cell. On the opposite, every cell center-VLP distance found below r_2 indicates that the VLP is inside the cell. We then plot the distribution of the distances ($n > 100$) for each different condition and plot the average value of the major axis, $r_1 = 17.6 \pm 3.7$ µm (mean ± sd) and the minor axis, $r_2 = 11.6 \pm 3.6$ µm (mean ± sd) of the different cells ($n = 16$) (Fig. 5C). In Fig. 5C, it is immediately seen that in absence of S, the average M(GFP)NE VLP-cell center distance is found between r_1 and r_2, both at 4 °C ($d = 13.4 \pm 3.2$ µm, mean ± sd) and at 37 °C ($d = 13.5 \pm 3.5$ µm), these mean values being not statistically different ($p = 0.98$, Mann Withney U test). For MNES VLP-M(GFP), at 4 °C, we observed a slight but statistically significant ($0.01 < p < 0.04$) decrease in the mean VLP-cell center distance ($d = 11.8 \pm 5$ µm) when compared to M(GFP)NE VLP. From Fig. 5C it can also be seen that, in this case, the distance distribution is widened and that some VLPs start to exhibit distances at values much below r_2, suggesting entry of these VLPs. This is confirmed when observing the M(GFP)NES VLP-cell center distance distribution at 37 °C. In this case the mean distance value is approximately divided by two ($d = 6.1 \pm 3.0$ µm) and is statistically strongly different from all the other distributions ($10^{-33} < p < 2.10^{-15}$) we established here. This clearly suggests that the presence of S on the surface of the VLPs induces a preferential endocytosis in A549-hACE2, cells carrying the hACE2 viral receptor.

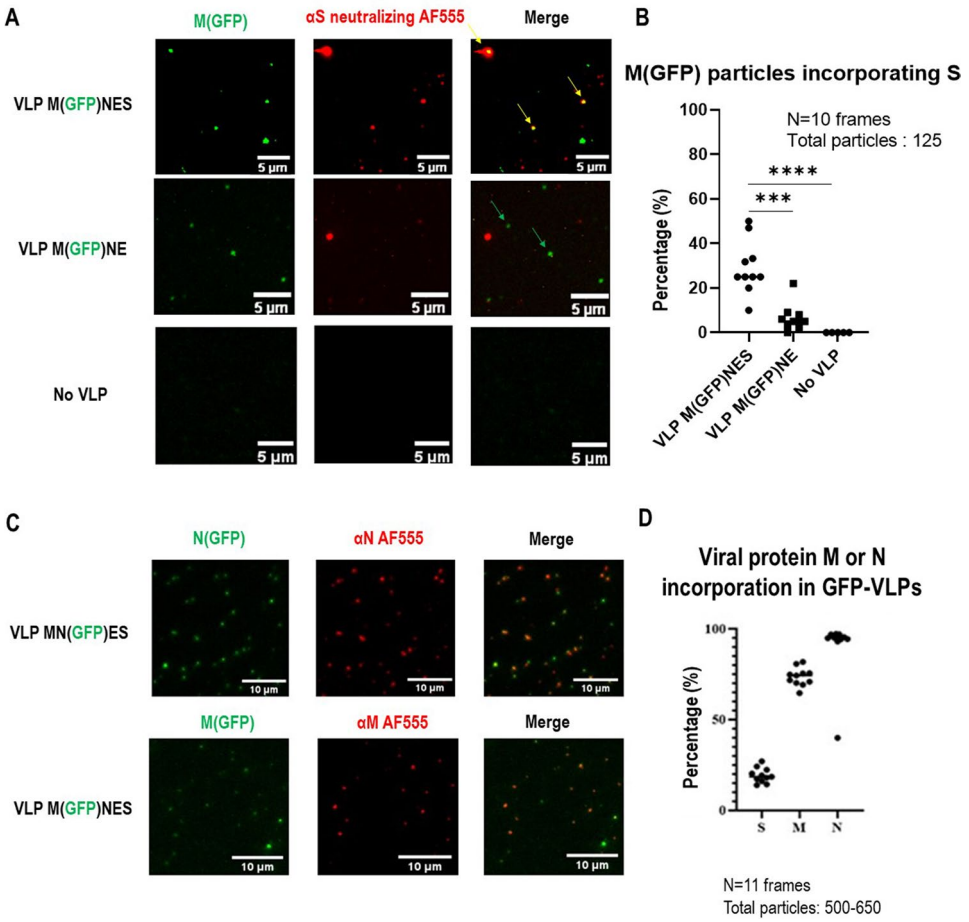

Figure 4. Evaluation of the incorporation of the Spike S, N and M in fluorescent SARS-CoV-2 VLPs using immuno-spotting coupled to TIRF-Microscopy. (**A**) TIRF images of M(GFP)NES VLPs, M(GFP)NE VLPs and control. An anti-S antibody coupled to a AF555 secondary antibody was used for S immunolabeling. Yellow arrows show the anti-S antibody-AF555 bound to VLPs-(GFP). Green arrows show VLPs-(GFP). Red arrows show antibody-labeled VLPs. The scale bar is 5 µm. (**B**) Percentage of S incorporation in M(GFP)NES versus M(GFP)NE and the control (no VLP). For each condition, 125 fluorescent particles were counted over 10 images (frames). One dot in the graph represents the % of S incorporation in the fluorescent VLP(M-GFP), i.e. % of colocalization in each frame. The t-test was calculated and the p-value between VLP M(GFP)NES and VLP M(GFP)NE is 0.0001 and p-value between VLP M(GFP)NES and No VLP is < 0.0001. (**C**) Images of SARS-CoV-2 M(GFP)NES and MN(GFP)ES VLPs as revealed by immuno-spotting coupled to TIRF-M, showing N or M incorporation in the MN(GFP)ES or M(GFP)NES VLP respectively with an anti-N or anti-M antibody coupled with an Alexa555 labeled secondary antibody, as indicated. The scale bar is 10 µm. (**D**) Quantification of the incorporation (%) of S, M or N on respective GFP-VLPs. N = 2, 11 images per sample and the number of particles counted was between 500 and 650 for each condition.

To confirm that this endocytosis was mediated by hACE2, we expressed in A549 cells a mScarlet1 tagged version of ACE2 and repeated the same experiment of M(GFP)NES VLPs internalization for 15 min at 37 °C on live cells. After fixation, z-projection imaging of M(GFP)NES VLPs in A549-hACE2mScarlet1 cells showed the internalization of the M(GFP)NES VLPs on the receptor ACE2. Z-projection imaging at 4 °C showed reduced internalization of the M(GFP)NES VLPs decorating the cell surface on the hACE2mScarlet1 receptor (Supplemental Fig. 5). The mScarlet1 versus GFP fluorescence emission is shown as a control (Supplemental Fig. 5A). Quantification of confocal images reveals that more than 65% of the GFP(+) dots were associated with the mScarlet1(+) dots (Supplemental Fig. 5B), reinforcing the idea that all the VLPs containing S were able to load on the ACE2 receptor at the cell surface of pulmonary cells mimicking hACE2-dependent SARS-CoV-2 endocytic entry. A colocalization of ~ 80% of the M(GFP)NES VLPs on the receptor hACE2mScarlet1 was observed (Supplemental Fig. 5C). In the absence of VLP, the cellular distribution of hACE2mScarlet1 remains diffuse (Supplemental Fig. 5D).

However, these above results are not indicative on the ability of the fluorescent (M-GFP)-VLP to mimic viral entry up to the fusion step of the VLP upon cell internalization. In order to explore that question, we used the fluorescent (N-GFP)-VLP internalization assay in A549 pulmonary cells with or without hACE2 receptor (Fig. 5D). The number of fluorescent VLP (ie "green" dots) per cell, suggested that VLP-(N-GFP) docking on the

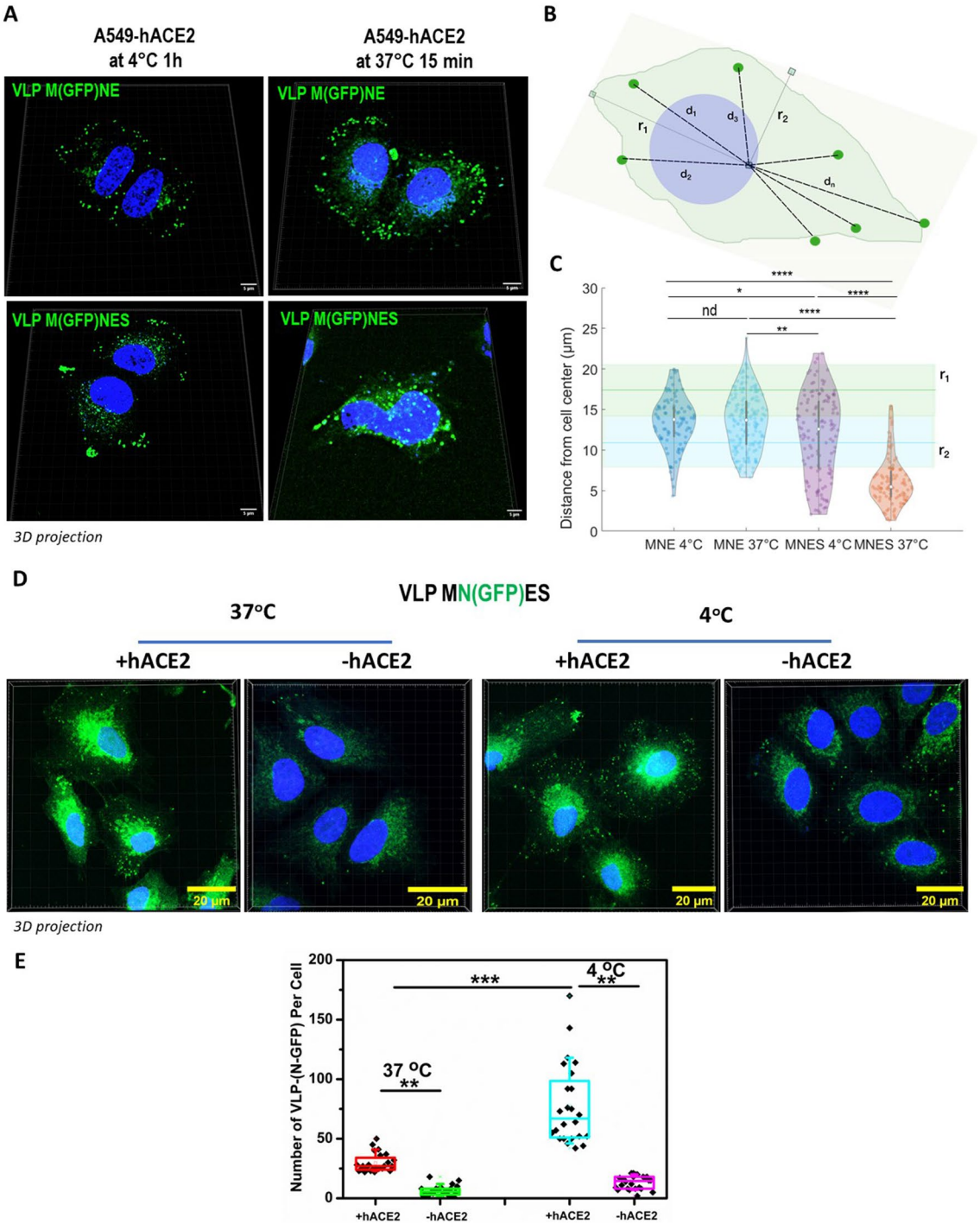

Figure 5. Internalization of VLPs-(GFP) with and without Spike on A549 pulmonary cells expressing or not hACE2 using confocal fluorescence microscopy. (**A**) M(GFP)NE ± S VLPs were incubated on A549-hACE2 cells at 37 °C for 15 min or at 4 °C for 1 h. Nuclei were stained with DAPI. (**B**) Schematic of distance measurement and cell center determination from minor and major axis of the cell. Scheme was drawn with the help of Inkscape. (**C**) Violin plot of the distribution of the VLP-cell center distances for the different conditions (MNE vs MNES at 4 °C and 37 °C respectively). The average value and the standard deviation of the major and minor axis (r_1 and r_2) observed in the different cell conditions (n = 16 cells) are respectively plotted as green and blue lines (mean) surrounded by rectangle (sd). All the conditions except MNES at 37 °C have distances mean values lying between these two limit axis values. *p-value < 0.05; **p < 0.01; ****p < 1.e10^{-15}; nd non significative. (**D**) Confocal images of MN(GFP)ES VLPs (in green) on A549 or A549-hACE2 cells incubated at 37 °C or at 4 °C show the internalization of VLPs. MN(GFP)ES VLPs were incubated on cells at 37 °C for 15 min or at 4 °C for 1 h. Nuclei were stained with DAPI (in blue). The scale bar is 20 µm. (**E**) Quantification of the number of MN(GFP)ES VLPs per cell in each condition, in the presence and the absence of the receptor hACE2 (+ or − hACE2) and at 4 °C (partially blocked endocytosis) or 37 °C (activate endocytosis and fusion). N = 2, 24 cells analyzed per condition. **p < 0.01; ***p < 0.001.

cells (at 4 °C) and VLP internalization (at 37 °C) were both significantly better in A549-hACE2 than A549 cells (respectively, at 4 °C, compare ACE2(+) 77.7 ± 33.3 versus ACE2(−) 13.2 ± 5.5 and at 37 °C, compare ACE2(+) 29.6 ± 7.6 versus ACE2(−) 6.4 ± 4.1 VLP per cell). Thus, efficient endocytosis of SARS-CoV-2 VLP containing S is highly hACE2 receptor-dependent. Secondly, the advantage of N-GFP is that it labels the viral core, and not the viral membrane as for M-GFP, allowing to monitor the disappearance of the VLP dots upon VLP internalization if viral fusion would occur. We thus compare the number of GFP dots (VLP) in A549hACE2 cells at 37 °C and 4 °C (mean value of 29.6 ± 7.6 at 37 °C versus 77.7 ± 33.3 VLP per cell at 4 °C, respectively): results show that more than half of the (N-GFP)-VLP dots «disappeared» upon entrance in the cells and N-GFP fluorescence concentrated near the nucleus; this difference between 37 and 4 °C suggests a possible fusion of the endocytosed (N-GFP)VLP within the cell (Fig. 5D) that would need to be proven by other complementary technics.

Discussion

As the SARS-CoV-2 pandemic persists around the world, it is necessary to further gather knowledge on this virus, especially in developing tools for studying virus assembly and virus entry in a safe BSL-2 environment (outside a BSL-3 and with non-infectious particles). Therefore, Virus-Like Particle production and characterization, if correctly mimicking the wild-type virus, would be essential to apprehend SARS-CoV-2 assembly mechanisms, and virus entry, in virology or to be used for the development of VLP-based vaccines in immunology. In this study, we established a minimal system for SARS-CoV-2 based VLPs production, requiring MNE/S with an optimized transfected plasmid ratio based on the RNAseq ratio measured in infected cells[17,18]. We show that the transfection and expression of individual M, N, E, or S alone are not sufficient to produce VLPs, as well as the combination of only two structural proteins. We conclude is that M, E, and N is the best condition, at a 3:12:2 ratio, required for optimal VLPs production (as shown by Kumar et al.[10] and Boson et al.[11]). We also observed that the addition of S reduces the incorporation of N and, to a lesser extent M (as seen by immunoblots, Fig. 1 and by dual color labeled VLP, Fig. 3) suggesting that the incorporation of the transmembrane Spike in the VLPs reduces N incorporation in favor of S. Moreover, S incorporation was favored in the optimized plasmid ratio and its maturation was much greater in the (N-GFP)VLP (Supplemental Fig. 3). Some of these findings could be in discordance with other studies. As a matter of fact, Xu et al.[5] showed that M alone can exit the cell, with this protein being the driver and M and E the minimal system. Indeed, in Fig. 1B, we can notice some M released from the transfected cells but nothing compare to the MNE combination. Plescia et al.[6] demonstrated that after being transfected alone, M is not present in the cell supernatant, as for M and E combination. However, they showed that the minimal requirement to obtain both proteins in the supernatant is to combine M with N. They also argue that the most efficient production is achieved with an M, N, and E combination, as the addition of E is playing an important role in particle assembly and release (see Bracquemond et al.[4]). In this study, the addition of S is not changing the proportion of M or N, which differs from Xu et al.[5]. Finally, other teams concluded that SARS-CoV-2 VLP production was sufficient when VLPs are based on M, E, and S combination in mammalian cells (Swann et al.[7]) or in insect cells (Mi et al.[8]). Our study shows that MN is required and that the addition of E makes the yield of VLPs production 2.5 fold better. A combination of M, N, and E was recently also reported for producing SARS-CoV-2 VLPs in plants (Moon et al.[9]) and previously in mammalian cells in the case of SARS-CoV[12,28]. Overall, it seems that the minimal optimal combination remains MNE/S to form SARS-CoV-2 VLPs. In addition, the formation of these VLPs did not required the presence of a packageable genomic RNA since all these VLPs were produced without. However, it is possible to introduce a pseudo-viral RNA inside the MNES VLPs as recently reported[29].

To optimize both VLPs formation and production, we performed an assay with an optimal ratio of the different structural proteins based on the viral RNA ratio coding for the 4 main structural proteins found in infected pulmonary Calu3 or intestine Caco2 cells[17] and in human pulmonary A549hACE2 cells[18]. Consequently, RNAseq data analysis allowed us to establish a plasmid ratio of 3:12:2:5 for M:N:E:S. This ratio increases VLPs production by 1.5 fold for MNE and MNES, as compared with the 3:3:3:5 ratio, with more S incorporation and more mature S2 on the VLP (Fig. 1C). We confirmed that particles analyzed by AFM were genuinely VLPs and rather not extracellular vesicles (Fig. 2C,D). To confirm that aspect, we checked one exosomal marker, CD81, using immune-spotting on GFP-VLP and confirm very low (less than 5%) or no colocalization between VLP and CD81(+) EVs (Supplementary Fig. 3). This suggests that SARS-CoV-2 VLPs are exiting through a secretory pathway that is different from EVs.

While Swann et al.[7] reported a 200 nm diameter and a height of 50–60 nm for MES VLPs using AFM, we measured a size of 126 ± 17 nm for MNES VLP using the same technique (Fig. 1D). No significant differences were observed between MNE, MNES and the wild-type virus (Lyonnais et al.[19]) by liquid AFM imaging. To confirm the size of these particles and to allow the study of SARS-CoV-2 using fluorescence and single molecule localization microscopy, we produced VLP incorporating M or N proteins in fusion with fluorescent or photo-convertible proteins. Using FCS and PALM, we found a 120-140 nm particle size range (Fig. 2D,E) : 100–110 nm for MNE VLPs, and 130 nm for MNES VLPs, which is consistent with AFM results (Fig. 1D). It is noticed that VLPs size are slightly bigger than wild-type virus particles as it has been described using AFM[19], TEM[19] or cryo-ET[27,30,31]. However, Spikes are difficult to observe: MNE and MNES VLP size could only be distinguished using FCS, where 2 populations were observed: one bigger than 100 nm in diameter, and one equal to 100 nm in diameter, suggesting that SARS-CoV-2 is producing some particles with and without Spikes as seen by immuno-spotting (Fig. 4). Using electron microscopy, Swann et al.[7] established a size around 130 nm while Xu et al.[5] obtained sizes between 70 and 90 nm depending on the cell lines used for VLPs production; Mi et al. reported around 100 nm[8] and Moon et al.[9] around 75 nm while we observed 90 nm for the wild-type virus[19]. These differences between our data and the ones from electron microscopy could arise from the dehydration process required during TEM sample preparation or from the absence of genomic RNA shaping the inside nucleocapsid N-RNA

core that might change particle assembly. The incorporation of other viral or cellular proteins could also be considered for tuning particle assembly. In another study, McMahon et al.[32] used high-throughput super-resolution microscopy to measure the size of the SARS-CoV-2 particles, showing that the virus's diameter distribution is mono-dispersed and centered at 143 nm. This size is in accordance with the one we found using FCS measurements of M(GFP)NES VLPs size in solution (Fig. 2D).

Labeling of VLPs with M Cter- and N Nter-tagged fluorescent proteins (Figs. 2 and 3), appeared possible only if there was a mixture of labeled and unlabeled M and N proteins for particle assembly. These could be very useful tools for visualizing virus assembly or entry into target cells as reported recently[6]. In addition, following double fluorescently labeled VLP could be an advantage in imaging VLP over time in different cell compartments or for imaging particle fusion upon cell entry, but would require to set up single particle tracking microscopy.

Concerning Spike incorporation in the VLP, thanks to the immuno-spotting technique on fluorescent VLPs with a neutralizing S antibody, we concluded that at least 25% of the M(GFP)NES VLPs incorporated the spike. This number might be underestimated due to the deposit of the MNES VLPs on the glass surface and to the affinity of the S antibody to the Spike, but it tends to support the observation that not all the VLPs produced by the mammalian cells are incorporating the spike. It would be interesting to vary the ratio of Spike expression in the productive cells to see if it changes the level of incorporation in the VLPs, and to try different anti-S neutralizing antibodies. Our results also suggest that the injection of MNES VLP mimicking the virus to animal models should provide adequate antibody responses without being infectious.

Finally, our study has shown that in the presence of overexpressed hACE2 receptors at the cell surface, M(GFP)NES VLPs can recognize the receptor and be endocytosed, confirming that the Spikes incorporated in the VLPs are functional in recognizing the receptor ACE2. Interestingly, a recent article[33] is demonstrating that this type of VLP can package viral RNAs to transduce and express genes in target cells, which reinforces the strong potential of SARS-CoV2 VLPs in vaccine development.

Overall, we report that the minimal system required for VLPs formation is M, N, and E structural proteins incorporating S and that VLPs can be optimized in production and maturation by mimicking SARS-CoV-2 mRNA ratio of infected cells. Tagging VLPs with fluorescent proteins was possible and could be very useful to image SARS-CoV-2-hACE2 internalization in host cells using single particle fluorescence quantitative microscopy. SARS-CoV-2 VLPs could be useful tools to study the viral life cycle of SARS-CoV-2 in a BSL-2 or as vaccine prototypes.

Data availability

The datasets of the humanized CoV-2 sequences generated during the current study are available in the GenBank repository with the ID number 2570843. The GenBank accession numbers for humanized SARS-CoV-2 protein nucleotide sequences used in this study are: BankIt2607198 hE(SARS-CoV2) OP095355, BankIt2607198 hM(SARS-CoV-2) OP095356, BankIt2607198 hN(SARS-CoV2) OP095358, BankIt2607198 hS(SARS-CoV2) OP095359.

Received: 26 March 2022; Accepted: 17 August 2022
Published online: 27 August 2022

References

1. Pushko, P. & Tretyakova, I. Influenza virus like particles (VLPs): Opportunities for H7N9 vaccine development. *Viruses* **12**, 518 (2020).
2. Gonelli, C. A., Khoury, G., Center, R. J. & Purcell, D. F. J. HIV-1-based virus-like particles that morphologically resemble mature, infectious HIV-1 virions. *Viruses* **11**, 507 (2019).
3. Kerviel, A. *et al.* Involvement of an arginine triplet in M1 matrix protein interaction with membranes and in M1 recruitment into virus-like particles of the influenza A(H1N1)pdm09 virus. *PLoS ONE* **11**, e0165421 (2016).
4. Bracquemond, D. & Muriaux, D. Betacoronavirus assembly: Clues and perspectives for elucidating SARS-CoV-2 particle formation and egress. *mBio* **12**, e02371 (2021).
5. Xu, R., Shi, M., Li, J., Song, P. & Li, N. Construction of SARS-CoV-2 virus-like particles by mammalian expression system. *Front. Bioeng. Biotechnol.* **8**, 862 (2020).
6. Plescia, C. B. *et al.* SARS-CoV-2 viral budding and entry can be modeled using BSL-2 level virus-like particles. *J. Biol. Chem.* **296**, 100103 (2021).
7. Swann, H. *et al.* Minimal system for assembly of SARS-CoV-2 virus like particles. *Sci. Rep.* **10**, 21877 (2020).
8. Mi, Y. *et al.* Production of SARS-CoV-2 virus-like particles in insect cells. *Vaccines* **9**, 554 (2021).
9. Moon, K.-B. *et al.* Construction of SARS-CoV-2 virus-like particles in plant. *Sci. Rep.* **12**, 1005 (2022).
10. Kumar, B. *et al.* Assembly and entry of severe acute respiratory syndrome coronavirus 2 (SARS-CoV2): Evaluation using virus-like particles. *Cells* **10**, 853 (2021).
11. Boson, B. *et al.* The SARS-CoV-2 envelope and membrane proteins modulate maturation and retention of the spike protein, allowing assembly of virus-like particles. *J. Biol. Chem.* **296**, 100111 (2021).
12. Siu, Y. L. *et al.* The M, E, and N structural proteins of the severe acute respiratory syndrome coronavirus are required for efficient assembly, trafficking, and release of virus-like particles. *J. Virol.* **82**, 11318–11330 (2008).
13. Floderer, C. *et al.* Single molecule localisation microscopy reveals how HIV-1 Gag proteins sense membrane virus assembly sites in living host CD4 T cells. *Sci. Rep.* **8**, 16283 (2018).
14. Inamdar, K. *et al.* Full assembly of HIV-1 particles requires assistance of the membrane curvature factor IRSp53. *eLife* **10**, e67321 (2021).
15. Arone, C. *et al.* Illuminating the nanoscopic world of viruses by fluorescence super-resolution microscopy. *Virologie* **25**, 47–60 (2021).
16. Inamdar, K., Floderer, C., Favard, C. & Muriaux, D. Monitoring HIV-1 assembly in living cells: Insights from dynamic and single molecule microscopy. *Viruses* **11**, 72 (2019).
17. Kim, D. *et al.* A high-resolution temporal atlas of the SARS-CoV-2 translatome and transcriptome. *Nat. Commun.* **12**, 5120 (2021).
18. Swain, J. *et al.* Reorganization of F-actin nanostructures is required for the late phases of SARS-CoV-2 replication in pulmonary cells. *bioRxiv* https://doi.org/10.1101/2022.03.08.483451 (2022).

19. Lyonnais, S. *et al.* Atomic force microscopy analysis of native infectious and inactivated SARS-CoV-2 virions. *Sci. Rep.* **11**, 11885 (2021).
20. Cardoso-Lima, R., Souza, P. F. N., Guedes, M. I. F., Santos-Oliveira, R. & Rebelo Alencar, L. M. SARS-CoV-2 unrevealed: Ultrastructural and nanomechanical analysis. *Langmuir* **37**, 10762–10769 (2021).
21. Chable-Bessia, C. *et al.* Low selectivity indices of ivermectin and macrocyclic lactones on SARS-CoV-2 replication in vitro. *COVID* **2**, 60–75 (2022).
22. Muller, P., Schwille, P. & Weidemann, T. PyCorrFit–generic data evaluation for fluorescence correlation spectroscopy. *Bioinformatics* **30**, 2532–2533 (2014).
23. Ovesný, M., Křížek, P., Borkovec, J., Švindrych, Z. & Hagen, G. M. ThunderSTORM: A comprehensive ImageJ plug-in for PALM and STORM data analysis and super-resolution imaging. *Bioinformatics* **30**, 2389–2390 (2014).
24. Levet, F. *et al.* SR-Tesseler: a method to segment and quantify localization-based super-resolution microscopy data. *Nat. Methods* **12**, 1065–1071 (2015).
25. Kiss, B., Kis, Z., Pályi, B. & Kellermayer, M. S. Z. Topography, spike dynamics, and nanomechanics of individual native SARS-CoV-2 Virions. *Nano Lett.* **21**, 2675–2680 (2021).
26. Ke, Z. *et al.* Structures and distributions of SARS-CoV-2 spike proteins on intact virions. *Nature* **588**, 498–502 (2020).
27. Laue, M. *et al.* Morphometry of SARS-CoV and SARS-CoV-2 particles in ultrathin plastic sections of infected Vero cell cultures. *Sci. Rep.* **11**, 3515 (2021).
28. Masters, P. S. The molecular biology of coronaviruses. *Adv. Virus Res.* **66**, 193–292 (2006).
29. Syed, A. M. *et al.* Rapid assessment of SARS-CoV-2–evolved variants using virus-like particles. *Science* **8**, 1626–1632 (2021).
30. Hardenbrook, N. J. & Zhang, P. A structural view of the SARS-CoV-2 virus and its assembly. *Curr. Opin. Virol.* **52**, 123–134 (2022).
31. Wu, H., Fujioka, Y., Sakaguchi, S., Suzuki, Y. & Nakano, T. Three-dimensional reconstruction by electron tomography for the application to ultrastructural analysis of SARS-CoV-2 particles. *Med. Mol. Morphol.* **55**, 60–67 (2022).
32. McMahon, A. *et al.* High-throughput super-resolution analysis of influenza virus pleomorphism reveals insights into viral spatial organization. *bioRxiv* https://doi.org/10.1101/2021.09.23.461536 (2021).
33. Syed, A. M. *et al.* Rapid assessment of SARS-CoV-2-evolved variants using virus-like particles. *Science.* **374**(6575), 1626–1632. https://doi.org/10.1126/science.abl6184 (2021).

Acknowledgements

We are grateful to Dr Olivier Schwartz (from Pasteur Institute, Paris, France) for the gift of the hACE2-mScarlet1 expression plasmid, and to Ms Virginie Sutter (Master student from Strasbourg University, France) for helping MG in VLP production, immuno-spotting and western blots. Confocal and TIRF microscopy were performed at the Montpellier Imaging Center for Microscopy (MRI) and the correlative fluorescence Atomic Force Microscopy at CEMIPAI CNRS Montpellier, France, which was funded by the REDSAIM program (Montpellier University).

Author contributions

M.G., C.A., P.M., D.B., J.S., A.M. and S.L. performed experiments. P.M. generated A549hACE2 and A549hACEm-Scarlet1 cell lines. M.G. directed VLPs production and purification, western blots, immuno-spotting, TIRF imaging and data analysis; SS generated M, N, E, S M(GFP) and M(Cherry) plasmids; D.B. generated N(mEOS2) and N(GFP) plasmids; C.A. and S.L. performed Bio-AFM and image analysis of VLPs; M.G. performed TIRF-M VLPs imaging and analysis; A.M. and C.F. performed live-VLPs fluorescence FCS and PALM microscopy study and analysis. D.M. and J.S. performed VLP-cell internalization using confocal microscopy and analyzed data. D.M. conceived, directed, and supervised the study. M.G. and D.M. wrote the manuscript. M.G., D.M., C.A., J.S., S.L. and C.F. edited the manuscript. S.S. and D.M. raised funding.

Funding

Drs Delphine Muriaux and Cyril Favard were funded by the "Centre National de la Recherche Scientifique" (CNRS, France), Montpellier University through a Montpellier University of Excellence (MUSE) grant and by the French Agency for Research (ANR COVID19) grant "NucleoCoV2". Pr Saveez Saffarian was funded by the National Science Foundation 2102948, and the 2 grants NSF58503110 and NSF58502848. M. Gourdelier is funded by the Region Occitanie France. A. Mouttou is the recipient of a CNRS PhD grant «CNRS 80 Prime». C. Arone is funded by the University of Montpellier, France. DM, SL and CF are members of the GdR Imabio CNRS consortium.

Competing interests

The authors declare no competing interests.

Additional information

Supplementary Information The online version contains supplementary material available at https://doi.org/10.1038/s41598-022-18681-z.

Correspondence and requests for materials should be addressed to D.M.

Reprints and permissions information is available at www.nature.com/reprints.

Publisher's note Springer Nature remains neutral with regard to jurisdictional claims in published maps and institutional affiliations.